Available online at www.sciencedirect.com
ScienceDirect
Journal of Catalysis 250 (2007) 313–323
JOURNAL OF CATALYSIS
www.elsevier.com/locate/jcat

# Gold supported on Cu–Mg–Al and Cu–Ce mixed oxides: An in situ XANES study on the state of Au during aerobic alcohol oxidation

Peter Haider, Jan-Dierk Grunwaldt, Ruth Seidel, Alfons Baiker *

*Institute for Chemical and Bioengineering, Department of Chemistry and Applied Biosciences, ETH Zürich, Hönggerberg, HCI, CH-8093 Zürich, Switzerland*

Received 6 June 2007; revised 9 July 2007; accepted 9 July 2007

**Abstract**

Liquid-phase in situ XANES experiments were used to elucidate the oxidation state of differently supported Au catalysts during the selective oxidation of 1-phenylethanol with molecular oxygen. The catalysts investigated included (i) Au(0.6 wt%)/$Cu_3Mg_3Al_2O_x$, (ii) Au(0.6 wt%)/$Mg_3AlO_x$, (iii) Au(2.9 wt%)/$CeO_2$, and (iv) a copper-doped analog, Au(0.6 wt%)/CuO–$CeO_2$ (20 wt% CuO). The XANES and EXAFS data were collected mainly in the fluorescence mode. Simultaneous determination of the structure (XANES) and the activity of the catalysts in the continuous-flow microreactor was achieved by following the oxidation state using XANES and the characteristic carbonyl vibration of the desired reaction product acetophenone using an IR spectrometer equipped with a transmission cell. Au/$Cu_3Mg_3Al_2O_x$ showed a small increase of conversion with time on stream accompanied by a slight reduction of the gold component. With Au/$Mg_3AlO_x$ and Au/CuO–$CeO_2$, a stronger reduction accompanied by increased catalytic activity was observed. The results of these mixed oxide-supported Au catalysts demonstrate that metallic gold is the main active species in catalytic aerobic alcohol oxidation. In contrast, a decrease in the product formation rate was observed for Au/$CeO_2$ with ongoing reduction. Results obtained from factor analysis indicate that the decrease in activity of the Au/$CeO_2$ with time on stream does not correlate with the much faster reduction of the catalyst and thus cannot be attributed to the increasing fraction of $Au^0$ species. This finding corroborates the importance of recording XANES spectra for structural identification simultaneously with online determination of the catalytic performance.


*Keywords:* In situ XANES; Gold; Mixed oxide supports; Oxidation state; Aerobic oxidation; Alcohol; 1-Phenylethanol; Chemometrics; Structure–performance relationship; Factor analysis

## 1. Introduction

Gold, being the noblest of all metals [1], had long been considered an inactive element in catalysis, despite early examples using Au catalysts in hydrogenation reactions [2–4]. However, over the last decade, Au has attracted increasing attention in the field of catalysis, as reflected in several reviews [5–9].

We have recently prepared a novel mixed-oxide-supported gold catalysts containing copper oxide as promoter for alcohol oxidation reactions [10]. Ex situ XANES investigations revealed that these catalysts contain gold in both reduced and oxidized states. In situ EXAFS measurements are needed to elucidate the effect of the oxidation state of Au on catalytic performance and to gain insight into the active Au species. Although such EXAFS measurements in the liquid phase have been little reported, gold catalysts have been the focus of recent EXAFS studies. EXAFS experiments have been used to establish a relationship between particle size and the interatomic Au–Au distance [11–14] and to characterize bimetallic systems [15–20]. The oxidation state of Au in CO oxidation has been the subject of various studies aimed at identifying the catalytically active species, with some reports emphasizing the importance of the metal being in a positive oxidation state [21–23] and, in contrast, other reports identifying zero-valent Au as the active species [5–7,24–28]. An alternative model emphasizing the interface of Au and the (oxidic) support was presented by Bond and Thompson [29]. Contradictory conclusions about the oxidation state of the active species of Au in the water–gas shift reaction catalyzed by Au catalysts also have been reported

* Corresponding author.
*E-mail address:* baiker@chem.ethz.ch (A. Baiker).

0021-9517/$ – see front matter 
doi:10.1016/j.jcat.2007.07.001

[30–36]. Calculations dealing with the origin of the activity of zero-valent Au nanoparticles in the low-temperature oxidation of CO indicate that the catalytic activity depends on the number of low-coordinated Au atoms [25,37,38] and that the support affects the shape of the particles, with oxygen defects being the crucial parameter [13,39,40]. However, most of the contributions analyzing the origin of Au as an active catalyst have dealt with gas-phase reactions, although the same question is important in liquid-phase alcohol oxidation as well [41].

Here we present in situ XANES experiments of the aerobic oxidation of an alcohol (1-phenylethanol) over differently supported Au catalysts. When identifying the oxidation state of Au, it was found that the white line of the Au $L_3$-edge, being an Au $2p_{3/2} \rightarrow 5d$ transition, increased with increasing oxidation state, leading to a shift toward lower energies [42]. Thus this apparent shift is a convolution of an intense pre-edge feature and the edge itself [43–46]. Due to the low gold concentration, including a strongly X-ray-absorbing matrix, most of the experiments were performed in fluorescence mode using a continuous-flow cell. Furthermore, the conversion was monitored online using an IR spectrometer equipped with a transmission cell [47] to correlate the catalytic performance and the oxidation state of Au.

## 2. Experimental

### 2.1. Preparation of supports and catalysts

The ternary $Cu_aMg_bAl_cO_x$- and the binary $Mg_3AlO_x$-mixed-oxide supports and the Cu-doped $CeO_2$ support were prepared by flame spray pyrolysis. $CeO_2$ was purchased from MCT Microcoating Technologies. The following notation is used throughout the article: $Cu_aMg_bAl_cO_x$[1], where the subscripts $a$, $b$, and $c$ indicate the molar ratio of Cu:Mg:Al = $a$:$b$:$c$. Detailed descriptions of the flame spray setup and the procedure applied can be found elsewhere [10,48,49]. In the next step, gold was deposited on the different binary and ternary mixed-oxide supports by deposition–precipitation following a procedure reported by Haruta [6]. Typically, about 1 g of the well-grinded support was suspended in 80 mL of deionized water and brought to pH 9–11 with freshly prepared 0.2 N NaOH. The catalyst was filtered off and dried at 80 °C for 18 h. A more detailed description of the preparation procedure is given elsewhere [10]. The Au loading of the catalysts was determined by means of AAS. The Au particle size in $Au/CeO_2$ was found to increase on exposure to reaction conditions due to reduction. The well-dispersed oxidized Au species present in the fresh sample resulted in reduced larger particles (5–10 nm) after reaction (as evidenced by HAADF-STEM, not shown). XRD measurements were carried out on a Siemens D5000 powder X-ray diffractometer using Cu$K\alpha$-radiation in the step scanning mode between 15° and 65° ($2\theta$), with a step size of 0.01° and 2 s per step.

[1] Note that the support contained significant amounts of carbonates due to the high partial pressure of $CO_2$ in the quenching zone of the flame, favoring the formation of carbonates.

### 2.2. In situ spectroscopic measurements

Experiments were performed at Hamburger Synchrotronstrahlungs-Labor (HASYLAB) at the Deutsches Elektronen-Synchrotron (DESY) using a Si(111) double-crystal monochromator (DORIS III, Beamline X1, 4.5 GeV, 140 mA injection current). An ionization chamber was used to determine the incoming X-ray intensity, and typically the Si(111) crystals were detuned slightly to 60% of the incoming intensity to remove higher harmonics. Due to the low loading of the noble metals and the strong X-ray absorption of the support, the experiments were performed in fluorescence mode. A 7-element Si(Li) fluorescence (Gresham) or 7-element Ge detector (Canberra) were used.

Catalysts monitored during the aerobic oxidation of 1-phenylethanol (20 mmol/L in toluene) to acetophenone were Au (2.9 wt%) on $CeO_2$ and Au (0.6 wt%) derived by deposition–precipitation on a mixed-oxide support of the nominal composition $Cu_3Mg_3Al_2O_x$. To further elucidate the role of Cu on the properties of the catalyst, Au(0.6 wt%)/$Mg_3AlO_x$ and Au(0.6 wt%) /CuO–$CeO_2$ (20 wt% CuO with respect to $CeO_2$) were analyzed using an identical method. The liquids were saturated with Ar, $O_2$, and $H_2$ and fed (at 0.3 mL/min) into the spectroscopic XAS cell via a peristaltic pump (ISMATEC ISM827). An IR spectrometer (BRUKER Tensor27, equipped with a DTGS detector) with a transmission cell was placed as close as possible to the measurement cell to minimize the dead volume for the online detection of conversion. Further details on the experimental setup can be found elsewhere [47,50]. The signal at 1690 $cm^{-1}$ [$\nu$(C=O) vibration of acetophenone] was selected to monitor the product formation. In addition, the signal at 1264 $cm^{-1}$ was used to verify the results obtained by analyzing the C=O stretching vibration. Note that the IR band at 1264 $cm^{-1}$ was assigned to a $\nu$(C–CO) vibration of the ring and the carbonyl-C; however, in all plots dealing with the catalytic performance, the signal at 1690 $cm^{-1}$ was applied. To ensure that baseline variations did not affect the shape of the signal, the intensity of bands not caused by acetophenone was analyzed. Variations in the baseline were found to be negligible with respect to the vibrational intensities of interest (1690 and 1264 $cm^{-1}$).

The XAS experiments were performed in fluorescence mode. Due to the absorption of the mixed-oxide support ($Cu_3Mg_3Al_2O_x$) containing a large quantity of incorporated Cu (Cu K-edge at 8979 eV), application of the transmission mode was not possible. This support, with a lower Cu content, was selected instead of the slightly different $Cu_5Mg_1Al_2O_x$ previously identified as somewhat more active in the aerobic oxidation of alcohols [10]. The latter support was unsuitable for recording XANES measurements in a reasonable time frame due to the extremely unfavorable signal-to-noise ratio. Note that measurement of a fluorescence spectrum of Au on the mixed-oxide support $Cu_3Mg_3Al_2O_x$ was made more difficult by the possible saturation of the detector caused by the Cu K-edge (Cu K-edge at 8979 eV; Cu$K\alpha_1$ and Cu$K\alpha_2$ fluorescence lines at 8046.3 and 8026.7 eV). Thus, a catalyst with a lower cop-

per concentration was chosen to allow recording of spectra of sufficient quality within a reasonable time frame.

But Au/$CeO_2$ allowed the collection of spectra in transmission mode along with the fluorescence spectra due to the higher Au loading. Scans were typically recorded at either 11,879–12,100 eV or 11,879–12,000 eV using a Si(111) crystal with step sizes of 1 eV around the edge and 2 eV above the Au $L_3$-edge. The data acquisition time was set to the appropriate time necessary (1–3 s per data point) and adapted for each individual sample. Note that the described differences in the experimental settings led to different times to collect the same number of spectra in the in situ experiments for the various samples. Different batches were prepared with components from varying sources.

At the beginning of each in situ experiment, spectra were obtained from the fresh catalyst at room temperature and at 80 °C with and without flowing Ar-saturated toluene. Afterwards, an $O_2$-saturated solution of 20 mmol/L 1-phenylethanol in toluene was admitted to the reaction chamber. Finally, $H_2$-saturated toluene was used to monitor a possible reduction of the compounds of interest.

### 2.3. Calculations

For a quantitative assessment of oxidized and zero-valent Au, factor analysis calculations were performed [51–53]. The basic hypothesis behind factor analysis is that a large data set ($D$) consists of only a limited number of $n$ components, and thus the large data set containing $r$ spectra each having $c$ data points can be reproduced by two matrices, with one ($S$) containing the spectra of the pure components and the other ($C$) containing the corresponding concentration profile, with $E$ representing the residual or error matrix [54,55],

$$D_{rc} = C_{rn} \cdot S_{nc}^{T} + E_{rc}. \quad (1)$$

Evolving factor analysis (EFA) [56,57] was used as an additional method for determining the number of components $n$ and generating an initial concentration matrix. Detailed overviews of the possibilities and applications of different factor analysis concepts are available elsewhere [54,55,58–60]. Here we have analyzed the spectra using the multivariate curve resolution with alternating least squares (MCR-ALS) approach [61–63]. The number of components (rank problem [58]) was determined by various methods, including the reduced eigenvalue ratio (REVR), calculation of the F-test and the corresponding significance level, and assessment of the (cumulated) variance represented by the eigenvector(s) as described previously [51]. The number of components $n$ was determined using EFA calculations and statistical tests. In EFA calculations, the eigenvalues $\lambda$ of the data matrix D were calculated $r$ times, with $r$ being the number of spectra in the initial data set [see Eq. (1)]. In such an evolutionary process, an eigenvalue emerged from the pool of eigenvalues attributed to noise when a new chemical species appeared and contributed to the enlarged data set. This analysis was performed in forward mode (starting from the first spectrum, then adding the second spectrum, the third spectrum, and so on) and backward mode [starting from the $r$th spectrum, then adding the $(r-1)$th spectrum, the $(r-2)$th spectrum, and so on]. The REV and the REVR represent the magnitude of the eigenvalues ($\lambda$) normalized with the size of the data matrix and the corresponding ratio of the $n$th and $(n+1)$th eigenvalues. Note that an eigenvalue was attributed to noise if the REV was small compared with the preceding value and similar to the following value and subsequently the REVR approached 1. When calculating the significance level (%SL), the null hypothesis ($H_0$: $\lambda = \lambda_{\mathrm{ERROR}}$) was accepted when %SL exceeded a certain level, typically 5%; otherwise, the null hypothesis was rejected, and the eigenvalue was considered significant [64]. In addition, the representation of the spectral features in the data set was calculated to elucidate the contribution of every single eigenvalue (variance and cumulative variance) [51].

All calculations were performed using Matlab 7.1. Software was either with a script downloaded from http://www.ub.es/gesq/mcr/ndownload.htm [65] or adapted from [51]. A nonnegativity constraint for both matrices—concentration profile and spectra of the pure components—was applied in the MCR-ALS calculation. Normalization of the spectra and simultaneous modification of the corresponding concentration profile was performed manually after the iteration. The initial concentration profile needed to start the MCR-ALS calculation was received from the results obtained by EFA: the first, second, third (and so on) forward curves were merged with the corresponding backward curve, with the smaller of the two corresponding eigenvalues always being retained [56]. Calculation of the EXAFS spectra was performed using the IFEFFIT (Version 0.8.049) [66] package and WinXAS 3.0 [67]. Note that the typical error in the determination of the coordination number was ±0.5 and ±0.02 Å in the interatomic distance.

## 3. Results

XANES spectra at the Au $L_3$-edge of the differently supported gold catalysts recorded during flowing Ar-saturated toluene through the microreactor cell are shown in Fig. 1. Whereas all catalysts exhibited Au in an at least partly positive oxidation state, the amount of oxidized Au species differed

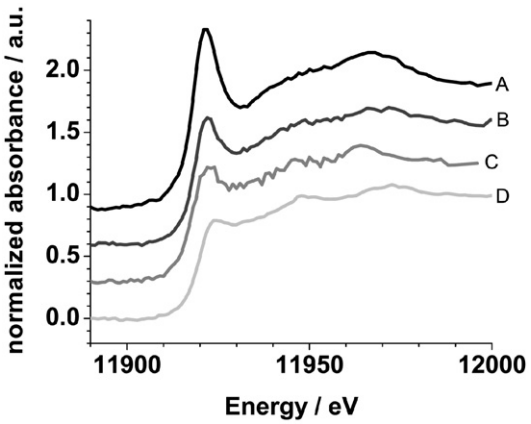


Fig. 1. XANES spectra at the Au $L_3$-edge of the fresh catalysts, recorded under flowing Ar-saturated toluene: (A) Au/$CeO_2$, (B) Au/CuO–$CeO_2$ (20 wt% CuO with respect to $CeO_2$); (C) Au/$Cu_3Mg_3Al_2O_x$, (D) Au/$Mg_3AlO_x$.

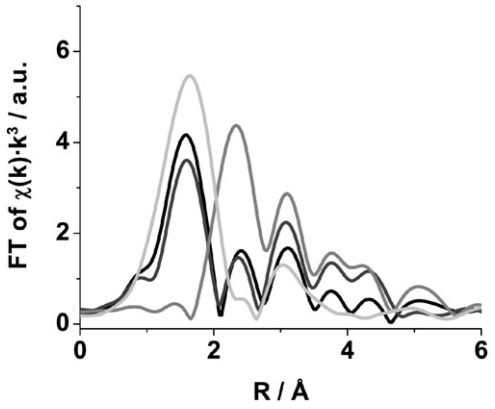


Fig. 2. Fourier transformed Au $L_3$-EXAFS spectra calculated ($k^3$-weighting, FT of $k = 2.6$–$8$ Å$^{-1}$) for the fresh (black line) and spent (dark gray) catalyst Au(0.6 wt%)/$Cu_3Mg_3Al_2O_x$. Metallic Au (Au foil, gray line) and $Au_2O_3$ (light gray) are plotted as references.

significantly. The two ceria-based catalysts exhibited a quite pronounced white line typical for $Au^{3+}$ species (Figs. 1A and 1B), whereas Au deposited on $Mg_3AlO_x$ and $Cu_3Mg_3Al_2O_x$ showed a lower fraction of oxidized Au.

EXAFS spectra of the fresh and spent Au/$Cu_3Mg_3Al_2O_x$ catalyst are presented in Fig. 2. The presence of Au in a positive oxidation state is indicated by an Au–O contribution appearing at $R = 1.6$ Å (not corrected for the phase shift), which decreased slightly during the aerobic oxidation of 1-phenylethanol. The Au–O distance in the catalyst was located at a similar value compared with that of $Au_2O_3$. In addition, metal particles were found in the fresh and spent catalyst; the Au–Au distance was similar compared with that found for an Au foil, indicating the simultaneous presence of Au in different oxidation states, possibly $Au^{3+}$ and $Au^0$. A closer look at the spectra reveals that the slight decrease in the Au–O contribution was accompanied by a slight increase in the Au–Au coordination number as indicated by the higher intensity of the Au–Au peak. The used catalyst exhibits a slightly larger Au–Au contribution and a slightly lower Au–O contribution compared with the fresh sample.

In situ spectra were first obtained at the Cu K-edge to determine the structure and oxidation state of Cu. No changes in the near-edge structure were detected when spectra of the fresh catalyst were compared with spectra recorded during the aerobic oxidation of alcohols or during flowing $H_2$-saturated toluene. Fig. 3 compares the XANES spectra of the fresh (Fig. 3a, A) and spent (Fig. 3a, B) catalysts to various reference materials, including $Cu(OH)_2$ (Fig. 3a, C), $Cu_2O$ (Fig. 3a, D), and metallic Cu (Fig. 3a, E). Based on the position of the main edge, it can be concluded that the copper was in the oxidation state $Cu^{2+}$. The characteristic sharp pre-edge pattern typical for $Cu^+$ components was missing, and the metallic copper exhibited a distinct post-edge pattern with characteristic oscillations leading to maxima at ≈9004 and ≈9026 eV. These peaks were absent in the post-edge patterns of the fresh and spent catalysts. These results are in good agreement with findings obtained from the catalytic testing of the pure supports. The supports were virtually inactive [10], in line with the observation that metallic Cu

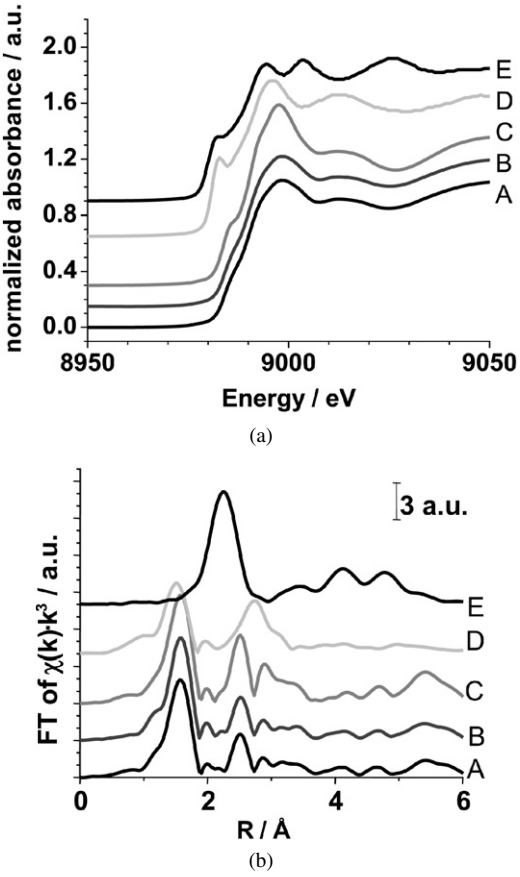


Fig. 3. (a) XANES spectra at the Cu K-edge and (b) corresponding Fourier transformed EXAFS spectra of the fresh (A) and spent (B) catalyst Au(0.6 wt%)/$Cu_3Mg_3Al_2O_x$. The reference components plotted here are: $Cu(OH)_2$ (C), $Cu_2O$ (D) and metallic Cu (Cu foil, E).

was the active species in the oxidation of alcohols [68] and that the copper species were present as $Cu^{2+}$. However, close similarity between the monitored catalyst and the near-edge structure of $Cu(OH)_2$ was observed. The XANES spectrum was not affected by in situ treatment of the sample; neither oxidation nor reduction of Cu was detected during the experiment. Thus, we presume that the promotional effect of Cu cannot be attributed to a redox cycle of the bulk Cu. Nonetheless, additional experiments may be needed with catalysts of lower copper content for a final assessment of the redox capability of the surface $Cu^{2+}$ species and their involvement in a possible redox mechanism.

To further characterize the Cu component in the catalyst, EXAFS spectra and XRD patterns were recorded. The radial distribution functions of the compounds are plotted in Fig. 3b. The contribution from the first oxygen shell was located at $R \approx 1.6$ Å, and the Cu–Cu scattering was at $R \approx 2.5$ Å for both the fresh and spent catalysts. Identical distances emerged from the analysis of the reference compound $Cu(OH)_2$. The reference $Cu_2O$ also exhibited an oxygen contribution at $R \approx 1.57$ Å but differed from the spectra of the catalyst in the Cu–Cu contribution; the EXAFS spectrum of $Cu^0$ is plotted for comparison. Similar to the XANES spectra, the EXAFS spectra recorded at the beginning and the end of the reaction showed similar features, indicating that the support was not affected by the in situ treatment.

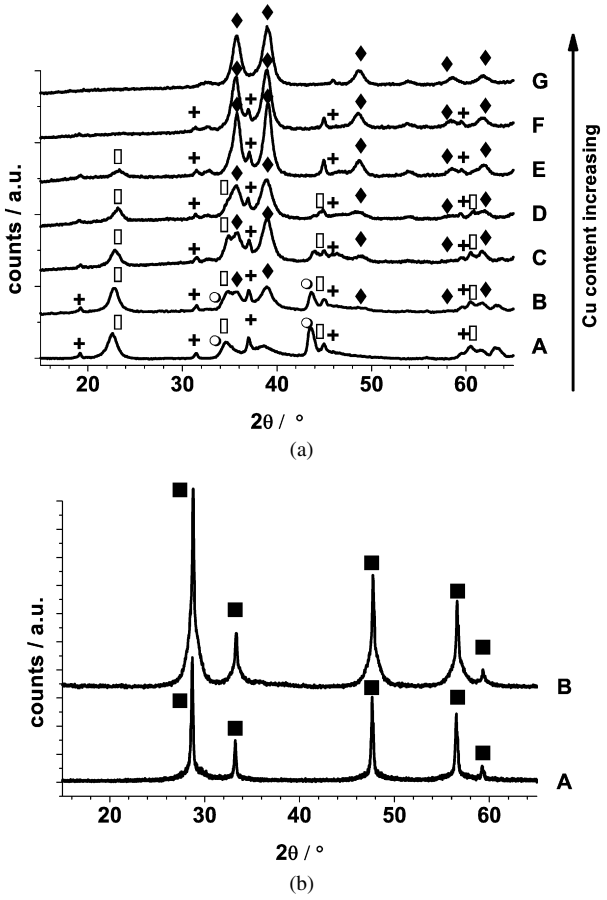


Fig. 4. (a) XRD patterns recorded for a series of $Au/Cu_aMg_bAl_cO_x$ catalysts. The Cu content is increasing from A to G with A containing no Cu and G containing no Mg: (A) $Au/Mg_3Al_1O_x$; (B) $Au/Cu_1Mg_5Al_2O_x$; (C) $Au/Cu_2Mg_4Al_2O_x$; (D) $Cu_3Mg_3Al_2O_x$; (E) $Cu_4Mg_2Al_2O_x$; (F) $Cu_5Mg_1Al_2O_x$; (G) $Au/Cu_3Al_1O_x$. (b) XRD patterns recorded for $Au/CeO_2$ (A) and $Au/CuO–CeO_2$ (B); symbols utilized: (+) spinel $(Mg,Cu)Al_2O_4$; (□) $Mg_6Al_2(OH)_{18}\cdot 4.5H_2O$; (○) $Al_2O_3$; (■) $CeO_2$; (◆) CuO.

XRD revealed four main phases in the $Au/Cu_aMg_bAl_cO_x$ catalyst (Fig. 4a). Note that the Cu-content increased from bottom to top in Fig. 4a while the ratio (Cu + Mg)/Al = 3 remained constant. $Al_2O_3$ was identified only in the samples with low Cu content. The dominant crystalline constituents were a mixed Mg–Al hydroxide $[Mg_6Al_2(OH)_{18}\cdot 4.5H_2O]$, a spinel, and a CuO phase. Due to the similarity in crystal structure, differentiation among $CuAl_2O_4$, $MgAl_2O_4$, and $Cu_xMg_{1-x}Al_2O_4$ $(0 < x < 1)$ was not possible. Fig. 4b depicts the XRD patterns recorded for $Au/CeO_2$ (Fig. 4b, A) and the corresponding Cu-modified analog (Fig. 4b, B) indicating that in this sample, no sign of the presence of crystalline CuO was found, not even when the corresponding area containing the largest CuO reflection ($34° < 2\theta < 40°$) was magnified. Pertinent reflections are listed in Table 1.

Applying the information obtained from the XRD patterns, fitting of the EXAFS spectrum recorded for $Au/Cu_3Mg_3Al_2O_x$ was attempted using the first Cu–O path and the first two Cu–Cu paths from a CuO input file. The result of this calculation is depicted in Fig. 5, indicating an excellent fit for the first two shells of the local environment of Cu. The results from the fitting procedure are listed in Table 2, and a comparison of the Cu–Cu and Cu–O distances of the selected paths in CuO and $Cu(OH)_2$ showed a difference well below 0.1 Å.

Table 1
Assignment of the XRD reflections obtained by means of XRD

| Phase | Assigned reflections | Phase | Assigned reflections |
|---|---|---|---|
| Spinel $(Mg,Cu)Al_2O_4$ (+) | 19° | CuO (◆) | 35.6° |
| | 31.4° | | 39.0° |
| | 37° | | 48.6° |
| | 45.1° | | 58.5° |
| | 59.5° | | 61.6° |
| $Mg_6Al_2(OH)_{18}\cdot 4.5H_2O$ (□) | 23.2° | $Al_2O_3$ (○) (corundum) | 35.1° |
| | 35° | | 43.2° |
| | 47.1° | | |
| | 60.7° | | |
| $CeO_2$ (■) | 28.7° | | |
| | 33.2° | | |
| | 47.7° | | |
| | 56.5° | | |
| | 59.2° | | |

The symbols used in Fig. 4 are (+) spinel $(Mg,Cu)Al_2O_4$; (□) $Mg_6Al_2(OH)_{18}\cdot 4.5H_2O$; (○) $Al_2O_3$; (■) $CeO_2$; (◆) CuO. The value denoted under assigned reflections refers to the Bragg angle $2\theta/°$.

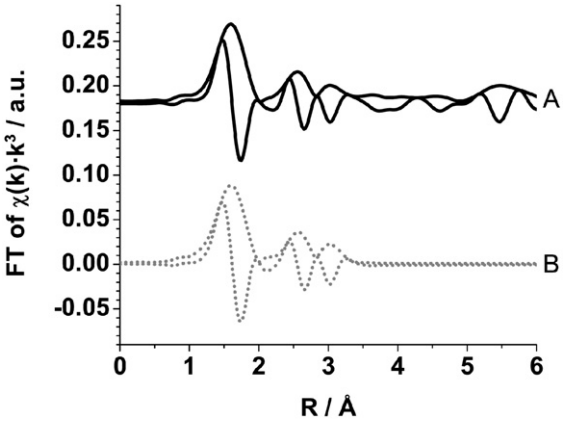


Fig. 5. Fitting of the EXAFS spectrum at the Cu K-edge ($Au/Cu_3Mg_3Al_2O_x$) using theoretical phase and amplitude functions calculated by the FEFF code. Black lines (A): measured spectrum, gray dotted lines (B): result from the fitting procedure. The residual of the fit was 4.6 (cf. Ref. [67]).

Table 2
Results from fitting the Cu K-EXAFS spectrum of $Au/Cu_3Mg_3Al_2O_x$

| Material | Path | $r$ (Å) | CN | $\sigma^2$ Å$^2$ | $\Delta E_0$ (eV) |
|---|---|---|---|---|---|
| $Au/Cu_3Mg_3Al_2O_x$ | Cu–O | 1.95 | 3.9 | 0.004 | 4.6 |
| | Cu–Cu | 2.93 | 2.8 | 0.007 | 11.8 |
| | Cu–Cu | 3.12 | 2.7 | 0.007 | 11.8 |

Path: Cu-backscatterer, $r$: interatomic distance; CN: coordination number; $\sigma^2$: Debye–Waller factor; $\Delta E_0$: shift of the energy threshold. The residual of the fit was 4.5.

After preparation, in the fresh state, a significant amount of oxidized Au atoms was found in both catalysts. To study the stability of the oxidized Au species, the $Au/Cu_3Mg_3Al_2O_x$ and $Au/CeO_2$ catalysts were heated in $O_2$ at 3 °C/min (Fig. 6). No reduction was observed for $Au/Cu_3Mg_3Al_2O_x$ during heating,

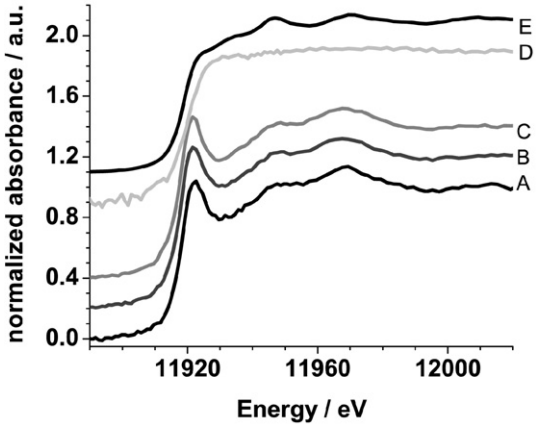


(a)

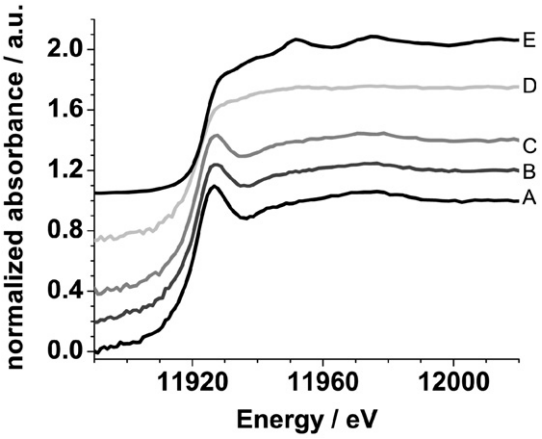


(b)

Fig. 6. (a) In situ XANES spectra at the Au $L_3$-edge during heating of (a) $Au/Cu_3Mg_3Al_2O_x$ and (b) $Au/CeO_2$ with 3 K/min in $O_2$ up to 350 °C, then switching to Ar followed by a change in the gas mixture to $H_2$. Assignment of the spectra: (A) room temperature, $O_2$ atmosphere, (B) 350 °C, $O_2$, (C) 350 °C, Ar, (D) 350 °C, $H_2$. The Au foil is plotted as a reference (E).

as indicated by the XANES spectrum. The fresh $Au/CeO_2$ catalyst exhibited a slightly higher intensity in the white line than $Au/Cu_3Mg_3Al_2O_x$. Also for this material, it was found that Au was not completely reduced even at elevated temperatures. Changing the gas mixture from $O_2$ to Ar at 350 °C did not significantly affect the oxidation state for both catalysts. However, complete reduction occurred readily after switching to $H_2$. Interestingly, the observed stability was much higher than was previously observed on such kind of catalysts [28].

Both the $CeO_2$- and $Cu_3Mg_3Al_2O_x$-supported Au catalysts were analyzed by means of in situ XANES. In both cases, the oxidation state of Au was not significantly affected by (a) heating up to 80 °C from room temperature or (b) flowing Ar-saturated toluene at 80 °C. Thus, in a next step, the reaction mixture (20 mmol/L $O_2$-saturated solution of 1-phenylethanol in toluene) was admitted to the reaction chamber. Results of the experiment performed with the $Au/Cu_3Mg_3Al_2O_x$ catalyst are depicted in Figs. 7a–7d. The rate of product formation (acetophenone) indicated by the intensity of the signal due to C=O stretching is shown in Fig. 7a. Interestingly, the rate of product formation increased slightly with time on stream, whereas only very little change was observed in the XANES spectra when comparing the spent Fig. 7b and fresh Fig. 7c catalysts. This indicates an unexpected high stability of the $Au^{3+}$ species under reaction conditions, consistent with the high stability of $Au^{3+}$ observed on heating in an oxygen atmosphere (Fig. 6a). However, the difference spectrum depicted in Fig. 7d demonstrates a slight reduction of the Au species. The high intensity of the white line, and thus the presence of $Au^{3+}$ species, also was preserved when the sample was treated with $H_2$-saturated toluene at 80 °C. A qualitatively similar behavior was observed when the Cu-free analog ($Au/Mg_3AlO_x$) was analyzed using the same sequence of experiments. However, in this case, the stability of $Au^{3+}$ was significantly lower compared with that of the Cu-doped sample ($Au/Cu_3Mg_3Al_2O_x$). Again, an increase in the catalytic activity was observed, accompanied by a continuous decrease in the intensity of the white line (spectra not shown).

The $Au/CeO_2$ catalyst was treated in a similar way, but it demonstrated distinctly different behavior. The reduction of the oxidized $Au^{3+}$ species occurred more rapidly, as shown by the sequence of spectra (A–J) in Fig. 8a. Again, spectra recorded at room temperature, at 80 °C, and during flowing Ar-saturated toluene at the same temperature (Fig. 8a, spectra A–C) did not demonstrate a significant influence on the catalyst structure due to this treatment. After the reaction mixture was admitted to the measurement cell, a fast and complete reduction was observed, as indicated by the disappearance of the white line and a distinct shift of the main edge by ≈+3 eV (Fig. 8a, spectra D–J). However, in contrast to the previously investigated catalysts, the activity (conversion) decreased almost linearly with time on stream, and the catalyst deactivated rapidly (Fig. 8b). Note that the rate of deactivation was much less pronounced during aerobic alcohol oxidation in a batch reactor [10]. Interestingly, the catalytic conversion of $Au/Cu_3Mg_3Al_2O_x$ was found to be higher than that of $Au/CeO_2$ in normal batch reactor experiments. This possibly results from better mixing in the slurry reactor where $O_2$ was bubbled through a liquid in a batch experiment compared with flowing an $O_2$-saturated liquid pumped through a continuous-flow cell [10]. An apparent divergence in the behavior of the two catalysts appeared as concerns the relationship between the oxidation state of Au and the catalytic performance. The conversion increased with a slight reduction of the gold species on $Au/Cu_3Mg_3Al_2O_x$, whereas it decreased with the extent of reduction on the $Au/CeO_2$.

In an attempt to resolve the apparent inconsistency emerging from straightforward analysis of the data measured in the in situ experiment of $Au/CeO_2$, factor analysis calculations were performed. It has been reported that $Au^{3+}$ reduces in a one-step process to $Au^0$ without an intermediate [28]; however, a simple linear combination of the corresponding XANES spectra did not turn out satisfactorily, because the spectra of metallic gold in a gold foil and oxidic gold in $Au_2O_3$ do not represent the spectra of small clusters as prepared in the present study [69]. Thus, factor analysis was applied to resolve the relative concentrations of oxidized and reduced Au species during the in situ experiment. EFA was used as to determine the number of components present in the data set. According to EFA calculations based on the data set in Fig. 8, the number of species present in

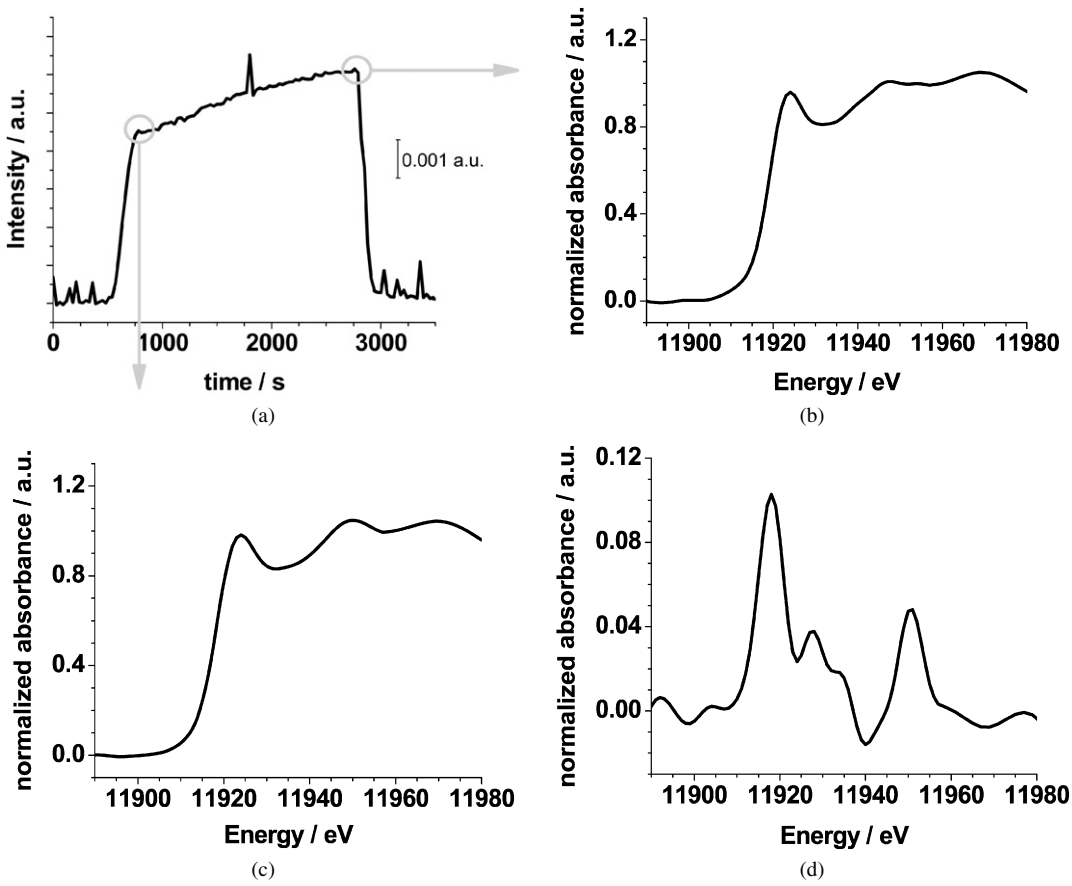


Fig. 7. In situ experiment on $Au/Cu_3Mg_3Al_2O_x$ with catalytic data by on-line FTIR spectroscopy and XANES spectra at the Au $L_3$-edge. An $O_2$-saturated solution of 1-phenylethanol (20 mmol/l) in toluene was fed to the catalyst (80 °C, 0.3 ml/min). The signal of the product acetophenone (FTIR, band $\nu = 1690\ cm^{-1}$) is depicted in (a), the corresponding XANES spectra at the end and at the beginning are depicted in (b) and (c). (d) Represents the difference spectrum between the fresh and used catalyst. Note that the sharp peak in (a) at 1800 s is an artifact caused by the mathematical spectra analysis.

the data set is $n = 2$, in agreement with previous results of a direct reduction to metallic gold [28]. Additional calculations and statistical tests were performed to verify the number of components (Table 3). The REVR value decreased abruptly from the second to the third eigenvalue with $REVR(\lambda_3) = \lambda_3/\lambda_4 \approx 1$, and the %SL distinctly exceeded the typical value of 5%; thus, the null hypothesis was accepted for the third eigenvalue. Finally, the variance in the data set was well represented in $\lambda_1$ and $\lambda_2$ (cumulative variance, 99.93%).

The results obtained from the MCR-ALS calculation are depicted in Fig. 9. The oxidized species showed high intensity in the white line, typical of $Au^{3+}$, accompanied by an apparent shift in the position of the main edge toward lower energy. The second (reduced) species exhibited similar features as metallic Au (Fig. 9b). The corresponding relative concentrations of the two species indicate that shortly after the admission of the reaction mixture ($t \approx 2000$ s) to the measurement cell, fast and complete reduction of the oxidized Au species occurred in a hyperbolic way (Fig. 9b). In contrast, the rate of product formation followed a nearly linear pattern. The decrease in conversion was detected even after the disappearance of oxidized Au species. Thus, we can conclude that the deactivation monitored in our EXAFS cell was not linked to the reduction step. To extract the correlation between the activity of the catalyst and the oxidation state of Au from other deactivation processes, $Au/CuO–CeO_2$ (20 wt% CuO with respect to $CeO_2$) was studied with the identical experimental setup. The spectra of the fresh and used sample are depicted in Fig. 10. It was found that doping with Cu significantly increased the rate of product formation in batch experiments, and, similar to $Au/CeO_2$, the catalyst was completely reduced after the fourth spectrum was recorded (Figs. 8 and 9). Reduction of the oxidized Au species in $Au/CuO–CeO_2$ (Fig. 11a) was even faster and led to reduced Au species shortly after the admission of the reaction mixture into the in situ cell. The steep increase in conversion at the starting point of the reaction was followed by a gradual increase (from 2300 to 3000 s), coinciding with the ongoing reduction of the Au species present in the sample. Subsequently, the conversion reached a plateau (Fig. 11b) with a constant white line intensity typical of $Au^0$, as shown in Fig. 11a.

## 4. Discussion

The in situ XAS and catalytic studies of the aerobic oxidation of 1-phenylethanol over differently supported ($Cu_3Mg_3Al_2O_x$ $Mg_3AlO_x$, 20 wt% $CuO/CeO_2$, and $CeO_2$) gold catalysts provided some interesting insight into the oxidation state of the gold component during the reaction. Although the samples behaved distinctly differently depending on the support, simul-

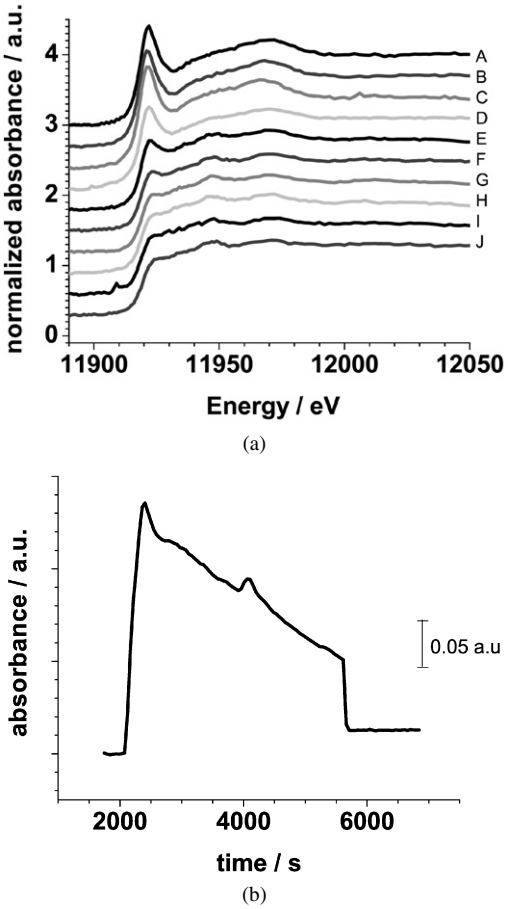


Fig. 8. In situ experiment on $Au/CeO_2$: (a) XANES spectra at the Au $L_3$-edge of: (A) dry sample, room temperature, (B) dry sample, 80 °C, (C) flowing Ar-saturated toluene at 80 °C, (D–J) flowing $O_2$-saturated 20 mmol/l 1-phenylethanol in toluene at 80 °C; (b) catalytic conversion of $Au/CeO_2$ determined by analyzing the reaction product acetophenone in a flow through cell by means of IR spectroscopy ($\nu = 1690\ cm^{-1}$). Note that the spike in conversion at 4100 s is an artifact presumably originating from flow instability (peristaltic pump).

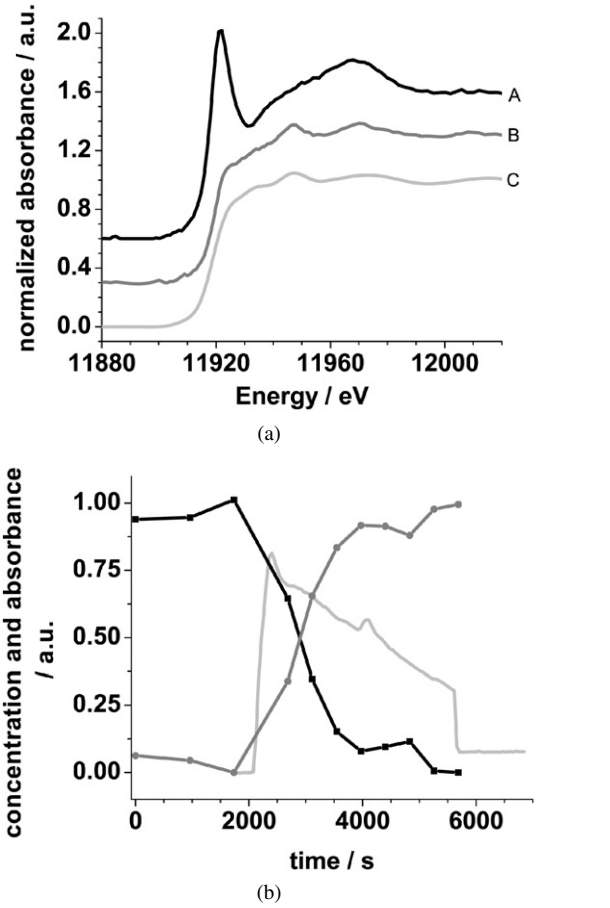


Fig. 9. (a) Spectra of the pure components obtained by means of evolving factor analysis utilizing the MCR-ALS approach; (A, B) components obtained by means of factor analysis calculations; (C) Au foil; (b) corresponding concentration profile with relative concentration of the oxidized species (black line, squares), of the reduced species (gray, bullets) and of the product acetophenone (light gray, magnified).

Table 3
Determination of the number of components present in the dataset obtained from monitoring $Au/CeO_2$

| $\lambda_n$ | $\lambda$ | REV | REVR | %SL | Variance | Cumulative variance |
|---|---|---|---|---|---|---|
| 1 | 880.84 | 0.641 | 145.4 | 1.06E−08 | 0.992 | 0.992 |
| 2 | 5.463 | 4.41E–03 | 50.184 | 1.06E−03 | 6.83E–03 | 0.999 |
| 3 | 0.097 | 8.78E–05 | 1.093 | 22.228 | 1.36E–04 | 0.999 |
| 4 | 0.078 | 8.04E–05 | 1.507 | 20.56 | 1.25E–04 | 1 |
| 5 | 0.045 | 5.33E–05 | 1.173 | 27.608 | 8.26E–05 | 1 |
| 6 | 0.033 | 4.55E–05 | 1.190 | 29.821 | 7.05E–05 | 1 |
| 7 | 0.023 | 3.82E–05 | 1.449 | 33.237 | 5.92E–05 | 1 |

The eigenvalues are sorted in decreasing order. The significance level (%SL) for accepting the null hypothesis was set to 5%.

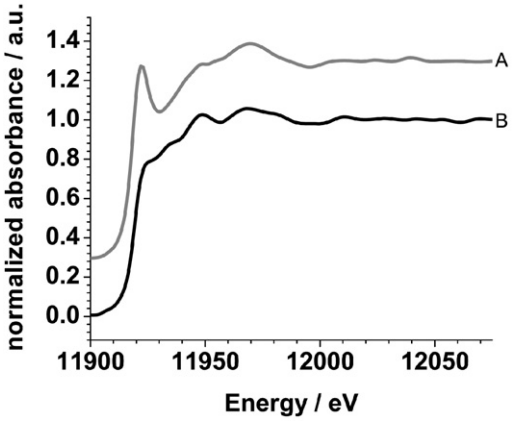


Fig. 10. Fresh (A, black) and spent (B, gray) XANES spectrum recorded for $Au/CuO–CeO_2$ (20 wt% CuO with respect to $CeO_2$) at the Au $L_3$-edge. The spectra were smoothed by applying a 3 point FFT filter.

taneous analysis of the oxidation state of Au and the catalytic conversion indicates that metallic Au probably was the dominant active species in the aerobic alcohol oxidation. Another interesting feature is the relatively high stability of the oxidized gold species during aerobic oxidation on $Cu_3Mg_3Al_2O_x$ compared with those on the other supports. Note that the present in situ XAS investigations were rather challenging due to the incorporation of strongly X-ray-adsorbing elements in the support ($CeO_2$) or, in case of Cu, due to the signal from the Cu K-edge located at 8979 eV and the corresponding fluorescence

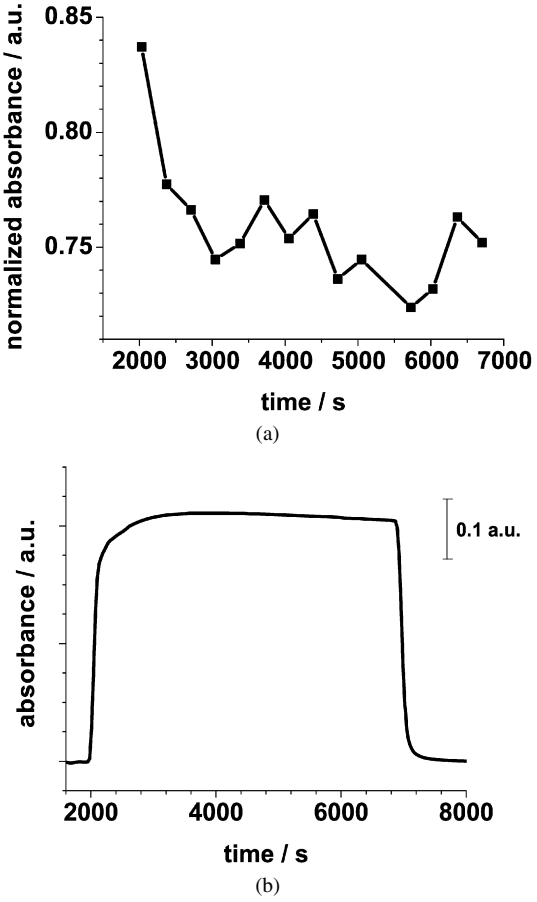


Fig. 11. (a) Intensity of the whiteline of gold during the in situ XANES experiment monitoring the Au/CuO–$CeO_2$ catalyst (20 wt% CuO with respect to $CeO_2$). The intensity plotted here represents the average normalized absorbance of 5 points forming the whiteline. (b) Catalytic conversion of Au/CuO–$CeO_2$ (20 wt% CuO with respect to $CeO_2$) determined by analyzing the reaction product acetophenone in a flow through cell by means of IR spectroscopy ($\nu = 1690\ cm^{-1}$).

lines at 8046.3 eV and 8026.7 eV (Cu$K\alpha_1$ and Cu$K\alpha_2$), which overlapped slightly with the Au $L_\beta$-fluorescence lines in the fluorescence spectra of the solid-state detector and may have saturated the energy-dispersive detectors. In addition, a low Au content was chosen to closely reproduce the conditions applied in the batch experiments. Consequently, the previous setup for transmission XAS measurements [47,50] in liquid phase was extended, and spectra were recorded in fluorescence mode with an energy dispersive detector.

Analysis of the EXAFS spectra obtained at the Cu K-edge and a successful fitting using Cu–O and Cu–Cu paths from CuO was in line with the CuO phase detected by XRD in the Cu-containing catalyst $Au/Cu_aMg_bAl_cO_x$. Both Cu-modified catalysts ($Au/Cu_3Mg_3Al_2O_x$ and Au/CuO–$CeO_2$) were more active than the nonpromoted catalysts, but differed significantly in terms of the diffraction pattern with respect to Cu; $Au/Cu_3Mg_3Al_2O_x$ contained crystalline CuO, which was not observed for Au/CuO–$CeO_2$ indicating that Cu does not have to be present in crystalline form.

As far as the effect of the promoter Cu on the oxidation state of Au is concerned, an inconsistent picture resulted from the analysis of the X-ray absorption data. Whereas the amount and stability of $Au^{3+}$ species were significantly greater in $Au/Cu_3Mg_3Al_2O_x$ compared with $Au/Mg_3AlO_x$; this effect was not observed in a comparison between Au/$CeO_2$ and Au/CuO–$CeO_2$ (20 wt% CuO with respect to $CeO_2$). The catalysts exhibited different initial amounts of oxidized Au and distinctly different characteristics regarding the oxidation state of Au during the catalytic aerobic oxidation of 1-phenylethanol. On $Cu_3Mg_3Al_2O_x$, Au maintained a positive oxidation state, unlike the previously studied $Pd/Al_2O_3$, in which Pd was reduced rapidly at 80 °C [47]. Also note the high stability of gold during the heating in air, which may indicate a strong gold–support interaction. Furthermore, $Au/Cu_3Mg_3Al_2O_x$ retained a significant amount of Au in oxidized form even in the presence of $H_2$-saturated toluene. Therefore, hydrogen formed during the dehydrogenation step probably would not be able to reduce the remaining oxidized Au species. This may be due to restricted accessibility or stabilization of the $Au^{3+}/Au^{+}$ species inside the matrix.

The simultaneous presence of both $Au^{3+}$ and $Au^0$ naturally complicates identification of the active species. However, comparing the first and last spectra (after longer time on stream) indicated a slight reduction accompanied by a slow increase in the catalytic conversion as determined by IR spectroscopy. On other supports ($Mg_3AlO_x$, $CeO_2$, and 20 wt% CuO/$CeO_2$), the $Au^{3+}$ species were less stable and reduced quickly after exposure to the reaction mixture (20 mM 1-phenylethanol in toluene saturated with $O_2$). In these catalysts, zero-valent Au was the only species detected during aerobic alcohol oxidation. In those cases, metallic gold must unequivocally play an active role in the dehydrogenation of the alcohols. In an attempt to test the activity of oxidized $Au^{3+}$ in the aerobic oxidation of alcohols, a homogeneous system was prepared using $HAuCl_4$ and $CuCl_2$ in aqueous phase. The concentrations were adjusted so that an identical Cu/Au ratio as in the heterogeneous catalyst was present; only the substrate/Au ratio was significantly lowered by 2 orders of magnitude to detect small turnover numbers. The experiment was also conducted using $HAuCl_4$ alone. However, none of the experiments detected any conversion under the reaction conditions applied in the heterogeneous catalyst systems.

The data obtained for Au/$CeO_2$ may appear to contradict this conclusion. Although Au was reduced, the conversion was decreased. However, the apparent contrast could be resolved by applying factor analysis calculations and comparing the population of oxidized and reduced species with the catalytic conversion. This analysis showed that the catalyst deactivation could not be traced back to the reduction of the catalyst and must have another origin. The deposition of carbonaceous species has been reported in Pt- and Pd-based catalysts [70]. Another reason for this may be the change in the support properties; it is well known that the basicity of the reaction mixture [71] and/or support [10,72] plays an important role in alcohol oxidation. The combined in situ XANES and FTIR study support the contention that metallic gold is the major active species in catalytic aerobic alcohol oxidation.

## 5. Conclusion

The oxidation state of gold particles deposited on different supports ($Cu_3Mg_3Al_2O_x$, $Mg_3AlO_x$, CuO–$CeO_2$, and $CeO_2$) was investigated during the liquid-phase catalytic aerobic oxidation of 1-phenylethanol using in situ XAFS combined with FTIR for product analysis. No systematic influence of CuO in the support on the oxidation state of Au was observed. However, for Au supported on the mixed-oxide $Cu_3Mg_3Al_2O_x$ oxidized gold species were present to a greater extent and were more stable than on $Mg_3AlO_x$. A correlation between the oxidation state of Au and catalytic activity was observed for Au/$Cu_3Mg_3Al_2O_x$, Au/$Mg_3AlO_x$, and Au/CuO–$CeO_2$. The 1-phenylethanol conversion increased with concomitant reduction of Au species and did not decrease even after the disappearance of oxidic species as evidenced by in situ XAS. Different behavior was observed for Au/$CeO_2$, with the activity decreasing simultaneously with the reduction of Au species. However, factor analysis calculations showed that the deactivation is not directly related to reduction of the gold species. Other factors, such as deposition of carbonaceous species, change of support, and interface properties (e.g., particle size, basicity), seem to be at the origin of the deactivation. Based on the results of the in situ XAS measurements on the mixed-oxide-supported gold catalysts, we propose that metallic gold is the active species in the aerobic liquid-phase alcohol oxidation.

The present study demonstrates that for multicomponent catalysts consisting of several species, simultaneous monitoring of structure and catalytic performance is essential to gain a rational basis for the derivation of structure–performance relationships, and advanced chemometrics is a valuable tool to help understand such relationships.

## Acknowledgments

The authors thank HASYLAB for offering beamtime for this project and the European Community Research Infrastructure Action under the FP6 "Structuring the European Research Area" program (through the Integrated Infrastructure Initiative "Integrating Activity on Synchrotron and Free Electron Laser Science," Contract RII3-CT-2004-506008) for financial support. They also thank Dr. Frank Krumeich for the electron microscopy investigations performed at the electron microscopy center of ETH Zurich (EMEZ), Drs. Gianluca Santarossa and Tamas Mallat for helpful discussions, the HASYLAB staff (Edmund Welter, Adam Webb, Mathias Herrmann) for assistance with measurements, and Stefan Marx, Bertram Kimmerle, Fabian Jutz, and Dr. Matteo Caravati for their help during the beamtimes.

## References

[1] B. Hammer, J.K. Nørskov, Nature 376 (1995) 238.
[2] D.A. Buchanan, G. Webb, J. Chem. Soc. Faraday Trans. 71 (1975) 134.
[3] R.P. Chambers, M. Boudart, J. Catal. 5 (1966) 517.
[4] P.A. Sermon, G.C. Bond, P.B. Wells, J. Chem. Soc. Faraday Trans. 75 (1979) 385.
[5] A. Haruta, Chem. Rec. 3 (2003) 75.
[6] M. Haruta, Cattech 6 (2002) 102.
[7] M. Haruta, M. Date, Appl. Catal. A 222 (2001) 427.
[8] G.C. Bond, D.T. Thompson, Catal. Rev. Sci. Eng. 41 (1999) 319.
[9] A.S.K. Hashmi, G.J. Hutchings, Angew. Chem. Int. Ed. 45 (2006) 7896.
[10] P. Haider, A. Baiker, J. Catal. 248 (2007) 175.
[11] A. Balerna, E. Bernieri, P. Picozzi, A. Reale, S. Santucci, E. Burattini, S. Mobilio, Surf. Sci. 156 (1985) 206.
[12] R.E. Benfield, D. Grandjean, M. Kroll, R. Pugin, T. Sawitowski, G. Schmid, J. Phys. Chem. B 105 (2001) 1961.
[13] N. Lopez, J.K. Nørskov, T.V.W. Janssens, A. Carlsson, A. Puig-Molina, B.S. Clausen, J.D. Grunwaldt, J. Catal. 225 (2004) 86.
[14] J.T. Miller, A.J. Kropf, Y. Zha, J.R. Regalbuto, L. Delannoy, C. Louis, E. Bus, J.A. van Bokhoven, J. Catal. 240 (2006) 222.
[15] H.M. Chen, R.S. Liu, K. Asakura, J.F. Lee, L.Y. Jang, S.F. Hu, J. Phys. Chem. B 110 (2006) 19162.
[16] Y.H. Chin, D.L. King, H.S. Roh, Y. Wang, S.M. Heald, J. Catal. 244 (2006) 153.
[17] L. Guczi, A. Beck, A. Horvath, Z. Koppany, G. Stefler, K. Frey, I. Sajo, O. Geszti, D. Bazin, J. Lynch, J. Mol. Catal. A Chem. 204 (2003) 545.
[18] M. Harada, K. Asakura, N. Toshima, J. Phys. Chem. 97 (1993) 5103.
[19] J. Radnik, L. Wilde, M. Schneider, M.M. Pohl, D. Herein, J. Phys. Chem. B 110 (2006) 23688.
[20] S. Hannemann, J.-D. Grunwaldt, F. Krumeich, P. Kappen, A. Baiker, Appl. Surf. Sci. 252 (2006) 7862.
[21] J.C. Fierro-Gonzalez, B.C. Gates, Catal. Today 122 (2007) 201.
[22] J. Guzman, B.C. Gates, J. Phys. Chem. B 106 (2002) 7659.
[23] G.J. Hutchings, M.S. Hall, A.F. Carley, P. Landon, B.E. Solsona, C.J. Kiely, A. Herzing, M. Makkee, J.A. Moulijn, A. Overweg, J. Catal. 242 (2006) 71.
[24] J.D. Grunwaldt, C. Kiener, C. Wögerbauer, A. Baiker, J. Catal. 181 (1999) 223.
[25] J.D. Grunwaldt, M. Maciejewski, O.S. Becker, P. Fabrizioli, A. Baiker, J. Catal. 186 (1999) 458.
[26] K. Okumura, K. Yoshino, K. Kato, M. Niwa, J. Phys. Chem. B 109 (2005) 12380.
[27] V. Schwartz, D.R. Mullins, W.F. Yan, B. Chen, S. Dai, S.H. Overbury, J. Phys. Chem. B 108 (2004) 15782.
[28] N. Weiher, E. Bus, L. Delannoy, C. Louis, D.E. Ramaker, J.T. Miller, J.A. van Bokhoven, J. Catal. 240 (2006) 100.
[29] G.C. Bond, D.T. Thompson, Gold Bull. 33 (2000) 41.
[30] Q. Fu, H. Saltsburg, M. Flytzani-Stephanopoulos, Science 301 (2003) 935.
[31] Q. Fu, W.L. Deng, H. Saltsburg, M. Flytzani-Stephanopoulos, Appl. Catal. B 56 (2005) 57.
[32] R. Burch, Phys. Chem. Chem. Phys. 8 (2006) 5483.
[33] C.H. Kim, L.T. Thompson, J. Catal. 244 (2006) 248.
[34] R. Leppelt, B. Schumacher, V. Plzak, M. Kinne, R.J. Behm, J. Catal. 244 (2006) 137.
[35] D. Tibiletti, A. Amieiro-Fonseca, R. Burch, Y. Chen, J.M. Fisher, A. Goguet, C. Hardacre, P. Hu, A. Thompsett, J. Phys. Chem. B 109 (2005) 22553.
[36] M.M. Mohamed, T.M. Salama, M. Ichikawa, J. Colloid Interface Sci. 224 (2000) 366.
[37] N. Lopez, T.V.W. Janssens, B.S. Clausen, Y. Xu, M. Mavrikakis, T. Bligaard, J.K. Nørskov, J. Catal. 223 (2004) 232.
[38] I.N. Remediakis, N. Lopez, J.K. Nørskov, Appl. Catal. A 291 (2005) 13.
[39] A.M. Kiss, M. Svec, A. Berko, Surf. Sci. 600 (2006) 3352.
[40] B.K. Min, W.T. Wallace, A.K. Santra, D.W. Goodman, J. Phys. Chem. B 108 (2004) 16339.
[41] T. Mallat, A. Baiker, Chem. Rev. 104 (2004) 3037.
[42] I.W. Bassi, F.W. Lytle, G. Parravano, J. Catal. 42 (1976) 139.
[43] I. Berrodier, F. Farges, M. Benedetti, M. Winterer, J.G.E. Brown, M. Deveughele, Geochim. Cosmochim. Acta 68 (2004) 3019.
[44] M.T. Coffer, C.F. Shaw, M.K. Eidsness, J.W. Watkins, R.C. Elder, Inorg. Chem. 25 (1986) 333.
[45] A. Pantelouris, G. Kuper, J. Hormes, C. Feldmann, M. Jansen, J. Am. Chem. Soc. 117 (1995) 11749.
[46] J.W. Watkins, R.C. Elder, B. Greene, D.W. Darnall, Inorg. Chem. 26 (1987) 1147.

[47] J.D. Grunwaldt, M. Caravati, A. Baiker, J. Phys. Chem. B 110 (2006) 9916.
[48] L. Mädler, H.K. Kammler, R. Müller, S.E. Pratsinis, J. Aerosol. Sci. 33 (2002) 369.
[49] L. Mädler, W.J. Stark, S.E. Pratsinis, J. Mater. Res. 17 (2002) 1356.
[50] J.D. Grunwaldt, C. Keresszegi, T. Mallat, A. Baiker, J. Catal. 213 (2003) 291.
[51] E.R. Malinowski, Factor Analysis in Chemistry, third ed., Wiley, New York, 2002.
[52] M. Fernández-García, Catal. Rev. Sci. Eng. 44 (2002) 59.
[53] M. Fernández-García, C. Márquez Alvarez, I. Rodríguez-Ramos, A. Guerrero-Ruíz, G.L. Haller, J. Phys. Chem. 99 (1995) 16380.
[54] A. de Juan, R. Tauler, Anal. Chim. Acta 500 (2003) 195.
[55] A. de Juan, R. Tauler, Crit. Rev. Anal. Chem. 36 (2006) 163.
[56] H. Gampp, M. Maeder, C.J. Meyer, A.D. Zuberbühler, Talanta 33 (1986) 943.
[57] M. Maeder, Anal. Chem. 59 (1987) 527.
[58] P. Geladi, Spectrochim. Acta Part B 58 (2003) 767.
[59] J.H. Jiang, Y. Ozaki, Appl. Spectrosc. Rev. 37 (2002) 321.
[60] T.H. Jiang, Y. Liang, Y. Ozaki, Chemometr. Intell. Lab. 71 (2004) 1.
[61] E.J. Karjalainen, Chemometr. Intell. Lab. 7 (1989) 31.
[62] P. Tauler, E. Casassas, Anal. Chim. Acta 223 (1989) 257.
[63] R. Tauler, Chemometr. Intell. Lab. 30 (1995) 133.
[64] E.R. Malinowski, J. Chemometr. 3 (1989) 49.
[65] J. Jaumot, R. Gargallo, A. de Juan, R. Tauler, Chemometr. Intell. Lab. 76 (2005) 101.
[66] B. Ravel, M. Newville, J. Synchrotron Rad. 12 (2005) 537.
[67] T. Ressler, J. Synchrotron Rad. 5 (1998) 118.
[68] F. Zaccheria, N. Ravasio, R. Psaro, A. Fusi, Chem. Eur. J. 12 (2006) 6426.
[69] D. Bazin, J.J. Rehr, J. Phys. Chem. B 107 (2003) 12398.
[70] C. Keresszegi, T. Burgi, T. Mallat, A. Baiker, J. Catal. 211 (2002) 244.
[71] L. Prati, M. Rossi, J. Catal. 176 (1998) 552.
[72] A. Abad, P. Concepcion, A. Corma, H. Garcia, Angew. Chem. Int. Ed. 44 (2005) 4066.